Temperature-dependence of the clear-sky feedback in radiative-convective equilibrium

Lukas Kluft[1,2,3], Sally Dacie[1,2], Manfred Brath[3], Stefan A. Buehler[3], and Bjorn Stevens[1]

[1]Max Planck Institute for Meteorology
[2]International Max Planck Research School for Earth System Modeling
[3] Meteorologisches Institut, Centrum für Erdsystem- und Nachhaltigkeitsforschung (CEN), Fachbereich Erdsystemwissenschaften, Universität Hamburg

Key Points:

- The temperature-dependence of the clear-sky radiative feedback saturates at $-1.2\,\mathrm{W\,m^{-2}\,K^{-1}}$
- Masking effects by water-vapor at the flanks of the CO_2 band weaken the radiative forcing at high column water vapor
- Barring insolation changes Earth's climate is stable to even unimaginably large increases in atmospheric CO_2.

Corresponding author: Lukas Kluft, `lukas.kluft@mpimet.mpg.de`

Abstract

We quantify the temperature-dependence of the clear-sky climate sensitivity in a one-dimensional radiative-convective equilibrium model. The atmosphere is adjusted to fixed surface temperatures between 280 K and 320 K while preserving other boundary conditions in particular the relative humidity and the CO_2 concentration. We show that an out-of-bounds usage of the radiation scheme RRTMG can lead to an erroneous decrease of the feedback parameter and an associated "bump" in climate sensitivity as found in other modelling studies. Using a line-by-line radiative transfer model, we find an almost constant longwave radiative feedback at surface temperatures above 300 K. However, the line-by-line simulations also show a slight decrease in climate sensitivity when surface temperatures exceed 310 K. This decrease is caused by water-vapor masking the radiative forcing at the flanks of the CO_2 absorption band, which reduces the total radiative forcing by about 18 %.

Plain Language Summary

The climate feedback parameter describes how the net radiative balance at the top of the atmosphere changes with surface temperature. The magnitude of the feedback parameter here depends on the current state of the climate system. For example, a warmer climate state is accompanied by a moister atmosphere which limits the climate feedback and hence increase climate sensitivity – which is the surface warming due to a doubling of CO_2. Other modelling studies have shown that the climate sensitivity will first increase in a warmer reference climate, but decrease again when surface temperatures exceed 310 K. In this study, we are using a reference radiative transfer model to show how the misuse of a simplified radiation scheme leads to this spurious signal in the estimation of the climate feedback parameter. In addition, we explain how changes in the H_2O and CO_2 concentrations influence the spectral distribution of both the feedback parameter and the radiative forcing.

1 Introduction

The state-dependence of the climate sensitivity is of great interest when studying climate change as it influences the interpretation of the proxy record (Manabe & Bryan, 1985; Kutzbach et al., 2013), historical temperature observations (Andrews, 2014; Gregory & Andrews, 2016), and the interpretation of differences among models (Bourdin et al., 2021). While many studies focus on cloud feedbacks due to changes in self-aggregation, cloud amount, or cloud height (Becker & Wing, 2020; Zelinka et al., 2020; Bony et al., 2016), there is a growing but still inconclusive literature on the seemingly simpler question of the clear-sky radiant response to warming.

Recent modelling studies, ranging from conceptual (Meraner et al., 2013), to cloud-resolving, models (Romps, 2020), find that after an initial decrease the magnitude of the clear-sky feedback parameter, λ, again increases at yet higher surface temperatures (T_s). This non-monotonicity manifests itself as a pronounced "bump", a maximum in the clear-sky climate sensitivity, $\mathcal{S}$, at $T_\mathrm{s} \approx 310\,\mathrm{K}$. Seeley and Jeevanjee (2021) describe a physical mechanism that explains the changing temperature-dependence of λ: when the rise of the temperature is tied to the rise of CO_2, the increased CO_2 broadens the spectral interval over which CO_2 is the dominant absorber, thereby coupling OLR in these spectral regions to the tropospheric temperature, and hence T_s in a way that leads to a more negative λ with warming. The work by Seeley and Jeevanjee (2021) provides an elegant physical explanation for the climate sensitivity "bump" in studies with varying CO_2 concentration (e.g. Romps, 2020) and in doing so shows how λ effectively depends on CO_2. However, their mechanism fails to explain a similar "bump" in $\mathcal{S}$ as temperature increases in constant-CO_2 simulations as in Meraner et al. (2013). Moreover, coupling temperature changes to CO_2, while physical, makes it difficult to separate the state-dependence of λ on T_s from its dependence on CO_2.

In this study, we calculate $\mathcal{S}$ as a function of a fixed T_s, for $T_\mathrm{s} \in [280\,\mathrm{K}, 320\,\mathrm{K}]$. After the atmosphere has equilibrated to the boundary conditions and the chosen T_s, the radiative feedback is computed as the change in OLR between simulations at increasing T_s (Section 2). Calculations were initially performed using a fast radiative transfer model (Mlawer et al., 1997), identical to that used in many climate modelling studies. To check the calculations of the more parameterized fast radiative transfer model, and to understand how the spectral forcing and feedback associated with a doubling of atmospheric CO_2 depends on temperature, we also perform calculations with a line-by-line model (Section 2). Our approach differs from earlier studies (Goldblatt et al., 2013; Kluft et al., 2019) in that the temperature profile and heating rates are allowed to interact. We find that qualitative errors from the fast radiative model become pronounced as T_s increases above $300\,\mathrm{K}$, and it over estimates the temperature-dependence of $\mathcal{S}$ by more than a factor of two as compared to the line-by-line model reference (Section 3).

Studies of the clear-sky feedback date back to Simpson (1928), who proposed that – in an atmosphere whose optical properties arise from a condensible species (water) – OLR decouples from T_s when the atmosphere becomes optically thick. Ingram (2010) brought these ideas to the attention of the climate community (in the meantime planetary scientists, initially unaware of Simpson's work, had come to similar conclusions) and concluded that if the water vapor concentration is a function of temperature only, a warming atmosphere will increases its optical thickness (and hence its emission height) in a way to maintain a constant emission temperature. For Earth's atmosphere this happens when $T_\mathrm{s} > 300\,\mathrm{K}$ (Goldblatt et al., 2013; Koll & Cronin, 2018). This decoupling was later (and independently) shown to underpin a limit to how much energy Earth's troposphere can radiate to space in the thermal infrared (Nakajima et al., 1992), with runaway (greenhouse) warming ensuing when the absorbed insolation exceeds this limit (Kasting, 1988; Nakajima et al., 1992; Goldblatt et al., 2013, 2017). These findings encourage the expectation that λ and hence $\mathcal{S}$ will increase monotonically with T_s, increasingly so for $T_\mathrm{s} > 310\,\mathrm{K}$, rather than to first increase and then decrease, as found by Meraner et al. (2013). Our line-by-line calculations show a different behavior: λ asymptotes to a constant, but negative value, with warming. To understand this behavior we quantify the magnitude of the radiative forcing ΔF from a CO_2 doubling. At moderate temperatures we find an increase in ΔF with surface warming, which is driven by higher emission temperatures in the center of the CO_2 band due to a deepening of the troposphere (Huang et al., 2016). At warm temperatures this trend is reversed and ΔF decreases. Together this leads to a reduction of $\mathcal{S}$ with warming. By considering the spectral response to warming and forcing (Section 4) we are able to understand this behavior, also in light of the earlier literature.

2 Methods and data

To analyze how the clear-sky climate sensitivity, $\mathcal{S}$, varies with surface temperature, T_s, we use the one-dimensional radiative convective model konrad (Dacie et al., 2019; Kluft et al., 2019) equilibrated at prescribed values of T_s between 280 K to 320 K with a fixed relative humidity of 80 % (see Appendix for a more detailed model description). Figure 1a shows the resulting temperature profiles as a function of atmospheric pressure p.

The RCE simulations are performed for CO_2 concentrations of 348 ppmv and 696 ppmv which allows us to compute the radiative forcing ΔF and the feedback parameter λ. We define ΔF at a given T_s as the difference in net radiation balance ΔN at the top of the atmosphere between these two CO_2 concentrations

$$\Delta F = \Delta N_{696\,\mathrm{ppmv}} - \Delta N_{348\,\mathrm{ppmv}} \tag{1}$$

The feedback parameter λ is defined as the change in ΔN between simulations at constant $CO_2 = 348\,\mathrm{ppmv}$ and different T_s

$$\lambda(T_\mathrm{s}) = \frac{\Delta N(T_\mathrm{s} + \Delta T) - \Delta N(T_\mathrm{s} - \Delta T)}{2\Delta T} \tag{2}$$

with surface temperature difference $\Delta T = 1\,\mathrm{K}$. With this approach, we can study the temperature-dependence of the radiative forcing ΔF, the climate feedback λ, and the resulting climate sensitivity $\mathcal{S} = -\Delta F/\lambda$.

To check our method we have also performed simulations with a coupled T_s and computed λ as the regression of ΔN over ΔT_s during a perturbed simulation. We find that the results are in very good agreement with those obtained using Equation 2. However, the strong temperature-dependence of λ makes the linear regression error-prone, which mostly manifests in spurious signals in the estimated effective forcing (y-intercept of the regression). Therefore, we opted for the well-established fixed SST approach.

Baseline simulations are performed using the Rapid Radiative Transfer Model for GCMs (RRTMG, Mlawer et al., 1997). RRTMG is a fast radiation scheme which uses the correlated-k method with precalculated lookup tables for computational efficiency. For line-by-line simulations we replace the RRTMG longwave radiative transfer calculations with calculations using the Atmospheric Radiative Transfer Simulator (ARTS, Eriksson et al., 2011; Buehler et al., 2018). ARTS represents the longwave radiative fluxes based on 32 768 equidistant frequency points (lines) between $10\,\mathrm{cm}^{-1}$ and $3250\,\mathrm{cm}^{-1}$ ($\Delta\nu = 0.1\,\mathrm{cm}^{-1}$). Explicitly resolving the spectrum of OLR later allows us to investigate conceptual ideas about the dependence of OLR on T_s in different spectral regions.

For the sake of simplicity and to facilitate comparisons with previous modelling studies we do not consider the effects of ozone. We have performed calculations in which ozone is allowed to change, and while the basic physics that we describe are not influenced by this elaboration, as λ becomes small the effect of ozone can become important. Quantitatively its influence is found to depend on the details of its representation, particu-

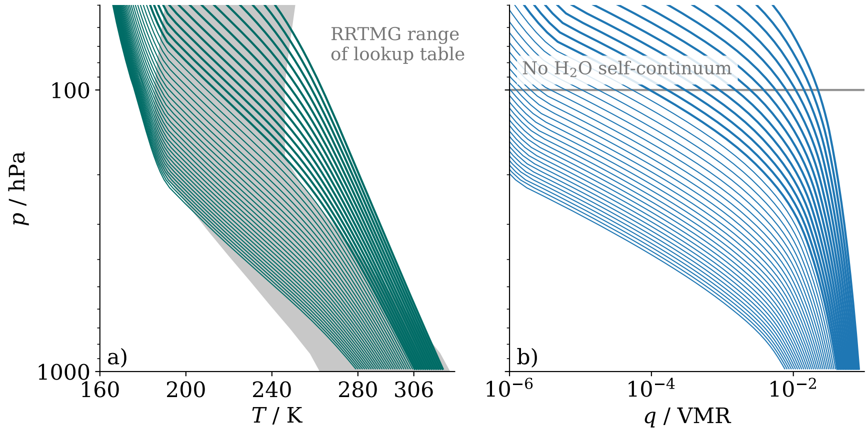

Figure 1. Equilibrium temperature *a)* and water-vapor volume mixing ratio *b)* profiles at different surface temperatures but constant CO_2 concentrations as a function of atmospheric pressure. The figure is clipped at 50 hPa to better visualize the troposphere. In addition, the RRTMG reference temperature range is shown as grey area.

larly in light of the deepening of the troposphere with warming, an interesting issue that we are beginning to explore together with experts on ozone chemistry.

The representation of the climate system, or even just the climate of the tropics, in terms of cloud (as well as aerosol and ozone) free radiative-convective equilibirum (RCE) is a strong, but common, simplification. The Charney (1979) report took it as a starting point and a large literature since then has found RCE solutions to be informative of how different physical processes influence climate sensitivity. For this reason RCE remains a well studied model problem (Popke et al., 2013; Stevens & Bony, 2013; Wing et al., 2017; Bourdin et al., 2021), one which for reasons elegantly articulated by Polya (1962), is worth first understanding.

Further information about konrad's configuration, RRTMG, and ARTS is given in the Appendix.

3 Temperature-dependence of the feedback parameter $\boldsymbol{\lambda}$

We run konrad for T_s between 280 K and 320 K to quantify the temperature-dependence of the feedback parameter

$$\lambda = f(T_\mathrm{s}; I, \alpha, \mathrm{RH}, \chi) \tag{3}$$

with constant values of insolation I, surface albedo α, relative humidity RH, and the gaseous composition χ. Seeley and Jeevanjee (2021) consider the related problem $\lambda = f(T_\mathrm{s}, \mathrm{CO}_2; ...)$, where the CO_2 concentration is variable.

For low temperatures, calculations based on RRTMG and ARTS agree well with one another. Figure 2 shows the radiative forcing ΔF and the feedback parameter λ (as defined in Section 2), as well as the resulting equilibrium climate sensitivity $\mathcal{S}$, as a function of T_s. Both results using RRTMG (grey), and the line-by-line radiative transfer model ARTS (green), show that λ (Figure 2b) increases from $-2.1\,\mathrm{W\,m^{-2}\,K^{-1}}$ to $-1.3\,\mathrm{W\,m^{-2}\,K^{-1}}$ as T_s increases from 280 K to 300 K. A more detailed feedback analysis (not shown) identifies this increase with the temperature-dependence of the water-vapor feedback.

For $T_\mathrm{s} > 300\,\mathrm{K}$, calculations with RRTMG result in a pronounced local maximum, or "bump", in $\mathcal{S}$. This is seen in Fig. 2, where $\mathcal{S}$ increases from less than 3 K at $T_\mathrm{s} = 300\,\mathrm{K}$ to about 8 K at $T_\mathrm{s} = 320\,\mathrm{K}$, and then rapidly decreases to less than 2 K at $T_\mathrm{s} = 320\,\mathrm{K}$. Fig. 2 further show that RRTMG's response can be attributed changes of the feedback parameter $\partial_{T_\mathrm{s}}\lambda$, rather than the forcing. Hence the bump, and its origins, are similar to what was found in other studies (Meraner et al., 2013; Romps, 2020) using correlated-k radiative transfer. When using ARTS, however, $\partial_{T_\mathrm{s}}\lambda$ does not increase. In contrast, the temperature-dependence of $\mathcal{S}$ begins to decreases at 305 K and λ converges to an almost constant value of $-1.2\,\mathrm{W\,m^{-2}\,K^{-1}}$.

RRTMG, and other fast-radiative transfer schemes, aggregate absorption features into bands, within which optical properties are calculated by interpolating across precomputed look-up tables. This reduces the computational intensity and speeds up the calculations many fold. In RRTMG the look up tables are based on an assumed atmospheric composition and thermal structure, close to those of the present-day Earth (Mlawer et al., 1997, their Sec. 3.2). As it turns out, how one interprets the word 'close' can be problematic. For instance, while RRTMG is documented to be valid for T_s as high as 320 K, this is based on a temperature profile representative of mid-latitude summer and assumes that there are no changes in the temperature lapse rate with increasing surface temperature (Mlawer et al., 1997, their Sec. 3.2). As a consequence, the temperature lapse-rate in the lookup table is larger than the moist-adiabat, which implies mid- and upper-tropospheric temperatures that are out of bounds at T_s above 306 K (see Figure 1). Popp et al. (2015) attempted to minimize the resultant errors by clipping the temperatures

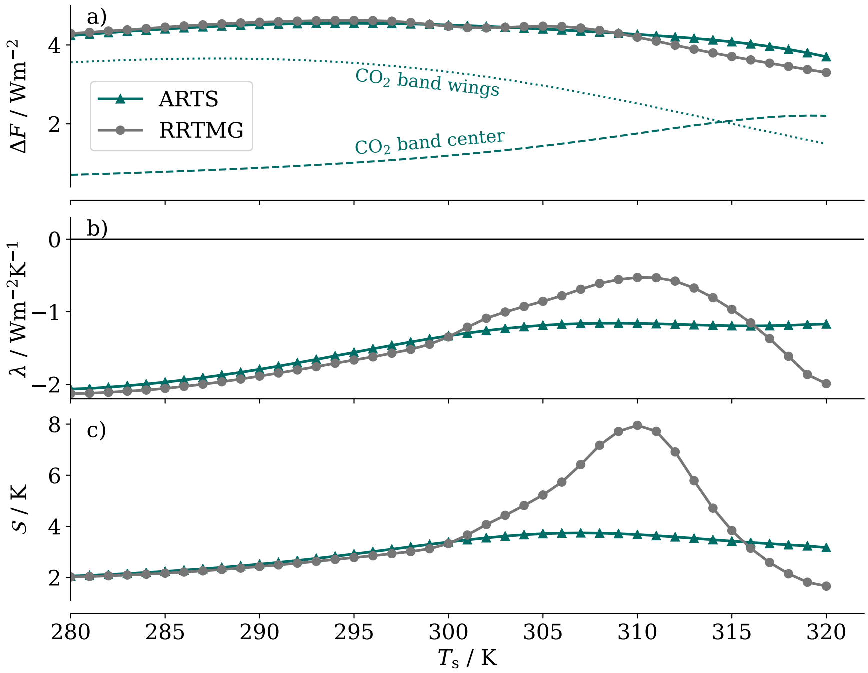

Figure 2. *a)* Effective radiative forcing ΔF, *b)* climate feedback parameter λ, and *c)* equilibrium climate sensitivity $\mathcal{S}$ as function of surface temperature T_s. All quantities are shown for experiments using the radiation scheme RRTMG (grey) and the line-by-line radiative transfer model ARTS (green).

to acceptable bounds when performing the gaseous look-up. The look-up tables are only one source of error. Another, which we identified, arises from RRTMG's calculation of the water-vapor self continuum. For computational expediency this is fit to only two reference values (at 260 K and 296 K) and is neglected entirely for pressures less than 100 hPa. This procedure is error prone as T_s increases above 296 K, the tropopause deepens, and when the window closes (which depends on relative humidity). For the case of RRTMG, these errors lead to an overestimation of OLR, which is misinterpreted as a decrease (more negative) of λ at high T_s. Coincidentally, this happens around the same temperature range at which the CO_2 mechanism described by Seeley and Jeevanjee (2021) begins to work.

In conclusion, using a line-by-line radiation model we find a robust increase of λ for T_s up to 305 K. Errors in the calculation of longwave irradiances by RRTMG are shown to be the cause of a spurious "bump" in $\mathcal{S}$. This "bump" looks similar, but is entirely unrelated, to the local maximum in $\mathcal{S}$ that Seeley and Jeevanjee (2021), find (and physically explain), when CO_2 is allowed to covary with T_s. For fixed CO_2, as T_s increases, λ asymptotes to a near-constant value of around $-1.2\,\mathrm{W\,m^{-2}\,K^{-1}}$. That the feedback becomes asypmtotically constant as the window closes is consistent with expectations from the literature on clear-sky radiative feedbacks in moist atmospheres (Ingram, 2010; Goldblatt et al., 2017). Its substantially negative value was less expected and has profound implications, something we address in more detail in the following section.

4 Spectral analysis of λ and ΔF

To understand why λ doesn't reduce to zero with warming, as one might expect based on a consideration of the response of water vapor alone to warming, we here examine the spectral feedback parameter λ_ν. This framework was used by Kluft et al. (2019) as well as Seeley and Jeevanjee (2021), and can also be used to study the role of different spectral regions in changing ΔF and $\mathcal{S}$. The important difference between our situation, and the situation envisioned by Simpson (1928), is that H_2O is not the only absorber in the infrared. Were that the case it would not be possible to force the system by increasing atmospheric concentrations of CO_2. The problem as we pose it here, is not how Earth can respond to energy accumulated by an external process, such as insolation or accretion of extra-planetary material (Abe & Matsui, 1988; Kasting, 1988; Nakajima et al., 1992), but rather how the reduction of infrared irradiance of the atmosphere can be compensated through warming.

The spectral feedback parameter λ_ν can be derived from our line-by-line calculations using Eq. (2). Figure 3b shows the smoothed λ_ν as a function of wavenumber ν for simulations at different temperatures (and hence absolute humidity). There is a strong temperature-dependence of λ_ν in the atmospheric window between $800\,\mathrm{cm}^{-1}$ and $1200\,\mathrm{cm}^{-1}$. This is driven by the increasing water vapor concentration in the warming troposphere, as λ_ν is indeed close to zero as soon as the atmosphere becomes fully opaque at high temperatures (darker blue shades) and stays close to zero for higher T_s. Hence, our results link the findings of Koll and Cronin (2018) with the studies by Nakajima et al. (1992) and Goldblatt et al. (2013).

In our simulations the total λ remains negative definite for all T_s. The thermal Planck feedback in the CO_2 bands around $667\,\mathrm{cm}^{-1}$ maintain a stable feedback with $\lambda \approx -1.2\,\mathrm{W\,m^{-2}\,K^{-1}}$. Adopting the analogy introduced by Seeley and Jeevanjee (2021), the infrared emission attributable to tropospheric CO_2 acts as a spectral radiator fin, stabilizing the climate to greenhouse forcing. This explains why a runaway greenhouse effect can not arise from the effect of CO_2 on thermal emission alone. The same mechanism which allows an increase in CO_2, or any other temperature independent greenhouse gas, to increase the radiative forcing, will also increase the radiative feedback of the system. Even in a constant CO_2 scenario, a moistening of the atmosphere will only dampen the thermal Planck feedback but never eliminate it. Ingram (2010) speculated that this might be the case, here we elaborate this thought and show that the ability of the atmosphere to maintain a feedback in some parts of the spectrum is intrinsically tied to the existence of a radiative forcing. In other words, if the system can be radiatively forced by a temperature-invariant greenhouse gas, i.e. CO_2, it also has the ability to maintain a stable climate.

Despite the constant value of λ, the magnitude of $\mathcal{S}$ decreases at $T_\mathrm{s} > 310\,\mathrm{K}$. This decrease in $\mathcal{S}$ is driven by a decrease of ΔF with warming. Usually, the radiative forcing is thought to increase with T_s (Huang et al., 2016). Such an effect is apparent in our simulations, but only for lower values of T_s, up to $300\,\mathrm{K}$ (Figure 2a). This strengthening of ΔF with warming arises from a larger contribution from the band center (between $620\,\mathrm{cm}^{-1}$ to $700\,\mathrm{cm}^{-1}$). At higher T_s, ΔF decreases, so that with $T_\mathrm{s} = 320\,\mathrm{K}$ it is $18\,\%$ less than its value at $295\,\mathrm{K}$. Fig 3 shows that the reduction in ΔF with warming is due to a weakening contribution from the edges of the $667\,\mathrm{cm}^{-1}$ CO_2 band. At $T_\mathrm{s} = 280\,\mathrm{K}$, $15\,\%$ of the forcing is carried by the band center, at $320\,\mathrm{K}$ the forcing from the band cen-

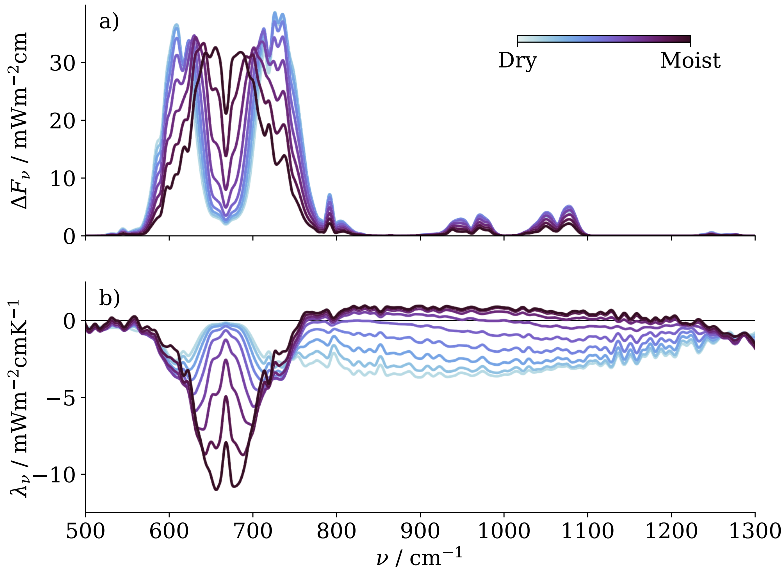

Figure 3. *a)* Spectral radiative forcing F_ν and *b)* spectral feedback parameter λ_ν as functions of wavenumber ν. Darker shades of blue represent a warmer and moister atmosphere. The spectra are smoothed using a $15\,\mathrm{cm}^{-1}$ running mean and zoomed to a range of $500\,\mathrm{cm}^{-1}$ to $1300\,\mathrm{cm}^{-1}$ to better resolve the CO_2 absorption band around $660\,\mathrm{cm}^{-1}$ and the atmospheric emission window between $800\,\mathrm{cm}^{-1}$ to $1200\,\mathrm{cm}^{-1}$. The actual line-by-line simulations cover a wavenumber range from $10\,\mathrm{cm}^{-1}$ to $3250\,\mathrm{cm}^{-1}$.

ter has increased more than three-fold and is responsible for 60 % of the total forcing (Figure 2a).

CO_2 absorption is so strong near the central absorption feature, that emission to space from these wavelengths originate in the stratosphere. Only lines whose emission height resides in the troposphere – where temperatures decrease with height – contribute to reduced emissions, and hence forcing from increasing CO_2 concentrations. As the tropopause rises with warming, an increasing fraction of the OLR originates from CO_2 in the troposphere, and its changes can contribute to the forcing. As increasing water vapor closes the window at $T_s > 300$ K, emission by H_2O increasingly dominates over emission by CO_2 on the flanks of the CO_2 band. This reduces the contribution of tropospheric CO_2 to the OLR, thereby reducing the contribution of its changes to forcing. The latter increasingly dominates at warmer temperatures, weakening ΔF from a doubling of CO_2 by about 18 % (from a value around 4.5 W m^{-2} to 3.7 W m^{-2}), consistent with an analytical model of the CO_2 forcing by Jeevanjee et al. (2020).

Seeley and Jeevanjee (2021) demonstrated how an increase in CO_2 concentration strengthens the CO_2 absorption band in the atmospheric window: at some point the CO_2 replaces H_2O as the dominant absorber and acts as a "CO_2 radiator fin". To understand the effects of warming on both λ and ΔF we find a different analogy helpful. We picture a "CO_2 archipelago in a developing, and eventually rising, sea of water-vapor absorption" (see Figure 4, the poetically inclined might think of these as Planckian outcroppings in a Simpsonian sea). From this point of view the share of the radiation that is emitted to space by H_2O in the troposphere, versus that from tropospheric CO_2 or from the surface, determines the strength of both λ and ΔF. As CO_2 concentrations rise, or the troposphere deepens, the CO_2 archipelago gains prominence – new islands even appear with rising CO_2 concentrations, as seen in Seeley and Jeevanjee (2021) – increasing the magnitude of both ΔF and λ. Warming of the atmosphere leads to the development of a "sea of absorption", which progressively reclaims the spectral landscape from CO_2 and the surface. This reduces ΔF for a given increase in CO_2 and progressively masks the ability of radiation from the "sea-floor" to escape to space. In our simulations, at $T_s = 320$ K the "absorption sea-level" is so completely determined by temperature, as evisaged by Simpson (1928), that the net radiative response to warming in the window region, $\nu > 767\,\mathrm{cm}^{-1}$, completely vanishes. At this point only the tallest mountains of

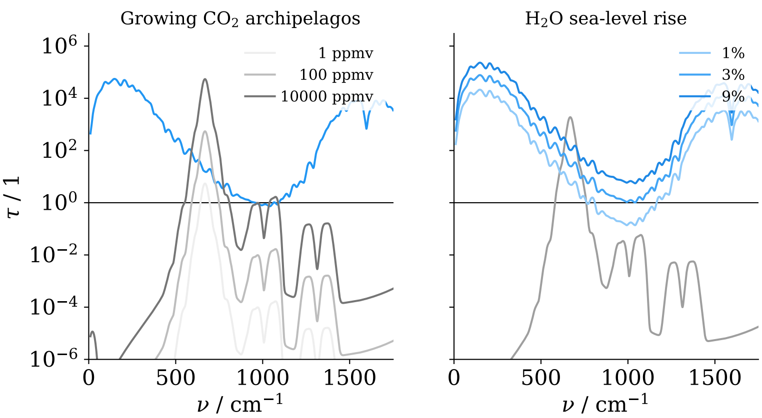

Figure 4. Optical thickness τ as a function of wavenumber ν. The left panel shows how the "CO_2 archipelagos" grow with an increase in atmospheric CO_2 concentration (darker greys). The right panel shows the rising "H_2O absorption sea-level" at higher water vapor volume mixing ratios (darker blues). In addition, the $\tau = 1$ line roughly indicates the location of opaque spectral regions ($\tau > 1$).

the "CO_2 archipelago", whose prominence is pronounced due to a rising tropopause, are left to balance an increase in forcing.

5 Conclusions

We perform calculations using the 1D-RCE model konrad at different surface temperatures T_s to analyze the temperature-dependence of the feedback parameter λ for a fixed CO_2 concentration. A line-by-line treatment of longwave radiant energy transfer (ARTS) is used to ensure an accurate computation of radiative fluxes and heating rates over a wide temperature range. By comparison to calculations with the RRTMG radiation scheme, we find that the use of the latter (albeit faster) scheme leads to increasingly erroneous results as surface temperatures increase beyond 300 K – errors in climate sensitivity are larger than a factor of two at 310 K. This is within the range of temperatures sampled by models with very high climate sensitivities subject to quadrupling of atmospheric CO_2. The erroneous behavior leads to a local maximum (or "bump") in the climate sensitivity, similar to what has been found in at least two other modelling studies (e.g. Meraner et al., 2013; Romps, 2020) using this same, or a similar, treatment of radiative transfer. The resulting "bump" of the climate sensitivity found in these studies looks similar to the one predicted by the "CO_2 radiator fin" mechanism by Seeley and Jeevanjee (2021), which arises from the strengthening of the Planck feedback from more pronounced CO_2 absorption features. In Romps (2020) both effects, the large increases in CO_2, which the climate sensitivity also depends on, and the RRTMG errors are conflated, and it is unclear which dominates.

Using ARTS, λ increases from $-2.1\,\mathrm{W\,m^{-2}\,K^{-1}}$ to $-1.2\,\mathrm{W\,m^{-2}\,K^{-1}}$ for T_s between 280 K and 305 K, which can be attributed to a progressive masking of the Planck feedback by increased water vapor absorption in the atmospheric window. In our simulations water vapor completely shuts the atmospheric window at T_s at 320 K, but already by 305 K this is balanced by a strengthening Planck feedback in the CO_2 absorption band. For $T_\mathrm{s} > 300\,\mathrm{K}$, λ becomes approximately independent of further increases in T_s examined in this study.

For $T_\mathrm{s} > 300\,\mathrm{K}$ the radiative forcing ΔF due to CO_2-doubling decreases by about 18 % from a value around $4.5\,\mathrm{W\,m^{-2}}$ to $3.7\,\mathrm{W\,m^{-2}}$. A spectral analysis of the radiative forcing reveals that this decrease is caused by increased water-vapor absorption which masks the radiative forcing at the flanks of the CO_2 absorption band.

To help conceptualize these effects we propose the picture of "CO_2 archipelagos in a sea of water-vapor absorption" to describe the subtle trial of strength between CO_2 and water-vapor absorption. This picture leads to the surprising result that as the atmosphere transitions to a moist greenhouse, CO_2 not only becomes less effective as a forcer, its presence also becomes a prerequisite for maintaining a negative atmospheric feedback. For these reasons the effect of increasing CO_2 concentrations on Earth's budget of terrestrial radiation alone is incapable of causing a runaway warming – for this to come to pass, clouds would have to cooperate.

Appendix A

Model configuration

We are using the 1D radiative-concective equilibrium model konrad (Kluft et al., 2021, v0.8.1). The boundary conditions are following Kluft et al. (2019) with a CO_2 concentration of 348 ppmv. The solar constant is set to $551.58\,\mathrm{W\,m^{-2}}$ at a zenith angle of 42.05° resulting in an insolation of $409.6\,\mathrm{W\,m^{-2}}$ (Wing et al., 2017; Cronin, 2014). The relative humidity in the troposphere is set to 80 % to ensure a reasonable amount of humidity in the upper troposphere, which is key for the interaction of lapse-rate and water-vapor feedbacks (Minschwaner & Dessler, 2004; Kluft et al., 2019). Above the cold-point tropopause the volume mixing ratio is kept constant.

Radiation scheme

We are using the Rapid Radiative Transfer Model for GCMs (RRTMG Mlawer et al., 1997) through the CliMT Python package. We have checked the radiative fluxes computed with CliMT-RRTMG and a stand-alone version and find that they agree within 1 %. RRTMG is a rapid radiation scheme and uses the distributed-k method for computational efficiency. This method requires precalculated lookup tables that are designed to span a wide range of atmospheric states.

Line-by-line treatment of radiation

We are using the Atmospheric Radiative Transfer Simulator (ARTS Eriksson et al., 2011; Buehler et al., 2018). ARTS is a line-by-line radiative transfer model and is used to calculate the longwave radiative fluxes using four emission angles (streams) and based on 32 768 equidistant frequency points between $10\,\mathrm{cm}^{-1}$ and $3250\,\mathrm{cm}^{-1}$ ($\Delta\nu = 0.1\,\mathrm{cm}^{-1}$). Gas absorption is based on the HITRAN database for gas species (Gordon et al., 2017) and additionally the MT_CKD model (Mlawer et al., 2012) for the continuum absorption of water vapor, CO_2, molecular nitrogen (all Version 2.52), and oxygen (Version 1.00).

Acknowledgments

Primary data is available on Zenodo through `https://zenodo.org/record/4565196`.

konrad v0.8.1 is available at `https://doi.org/10.5281/zenodo.4434837`, and the latest development version can be found at `github.com/atmtools/konrad`.

The research is supported by public funding to the Max Planck Society and through the European Union's Horizon 2020 Research and Innovation programs (Grant 820829, to the CONSTRAIN Project).

With this work we contribute to the Cluster of Excellence "CLICCS—Climate, Climatic Change, and Society" (EXC 2037, Project Number 390683824), and to the Center for Earth System Research and Sustainability (CEN) of Universität Hamburg.

The authors would like to thank the ARTS community.

References

Abe, Y., & Matsui, T. (1988, November). Evolution of an Impact-Generated H2O–CO2 Atmosphere and Formation of a Hot Proto-Ocean on Earth. *Journal of the Atmospheric Sciences*, *45*(21), 3081–3101. doi: 10.1175/1520-0469(1988)045⟨3081:EOAIGH⟩2.0.CO;2

Andrews, T. (2014). Using an AGCM to Diagnose Historical Effective Radiative Forcing and Mechanisms of Recent Decadal Climate Change. *Journal of Climate*, *27*(3), 1193–1209. doi: 10.1175/JCLI-D-13-00336.1

Becker, T., & Wing, A. A. (2020). Understanding the Extreme Spread in Climate Sensitivity within the Radiative-Convective Equilibrium Model Intercomparison Project. *Journal of Advances in Modeling Earth Systems*, *12*(10). doi: https://doi.org/10.1029/2020MS002165

Bony, S., Stevens, B., Coppin, D., Becker, T., Reed, K. A., Voigt, A., & Medeiros, B. (2016). Thermodynamic control of anvil cloud amount. *Proceedings of the National Academy of Sciences*. doi: 10.1073/pnas.1601472113

Bourdin, S., Kluft, L., & Stevens, B. (2021). Dependence of Climate Sensitivity on the Given Distribution of Relative Humidity. *Earth and Space Science Open Archive*, 13. Retrieved from `https://doi.org/10.1002/essoar.10506044.1` doi: 10.1002/essoar.10506044.1

Buehler, S. A., Mendrok, J., Eriksson, P., Perrin, A., Larsson, R., & Lemke, O. (2018). ARTS, the atmospheric radiative transfer simulator — version 2.2, the planetary toolbox edition. *Geoscientific Model Development*, *11*(4), 1537–1556. doi: 10.5194/gmd-11-1537-2018

Charney, J. G., Arakawa, A., Baker, D. J., Bolin, B., Dickinson, R. E., Goody, R. M., ... Wunsch, C. I. (1979). *Carbon dioxide and climate: a scientific assessment* (Tech. Rep.).

Cronin, T. W. (2014). On the choice of average solar zenith angle. *Journal of the Atmospheric Sciences*, *71*(8), 2994–3003. doi: 10.1175/JAS-D-13-0392.1

Dacie, S., Kluft, L., Schmidt, H., Stevens, B., Buehler, S. A., Nowack, P. J., ... Birner, T. (2019). A 1D RCE study of factors affecting the tropical tropopause layer and surface climate. *Journal of Climate*, *32*(20), 6769–6782. Retrieved from `https://doi.org/10.1175/JCLI-D-18-0778.1` doi: 10.1175/JCLI-D-18-0778.1

Eriksson, P., Buehler, S. A., Davis, C. P., Emde, C., & Lemke, O. (2011). ARTS, the atmospheric radiative transfer simulator, version 2. *Journal of Quantitative Spectroscopy and Radiative Transfer*, *112*(10), 1551–1558. doi: 10.1016/j.jqsrt.2011.03.001

Goldblatt, C., Kavanagh, L., & Dewey, M. (2017). The palaeoclimate and terrestrial exoplanet radiative transfer model intercomparison project (PALAEOTRIP): experimental design and protocols. *Geoscientific Model Development*, *10*(11), 3931–3940. doi: 10.5194/gmd-10-3931-2017

Goldblatt, C., Robinson, T. D., Zahnle, K. J., & Crisp, D. (2013). Low simulated radiation limit for runaway greenhouse climates. *Nature Geoscience*, *6*(8), 661–667.

Gordon, I. E., Rothman, S., Hill, C., Kochanov, R. V., Tan, Y., Bernath, P. F., ... Zak, E. J. (2017). The HITRAN2016 molecular spectroscopic database. *Journal of Quantitative Spectroscopy and Radiative Transfer*, *203*, 3–69. doi: 10.1016/j.jqsrt.2017.06.038

Gregory, J. M., & Andrews, T. (2016). Variation in climate sensitivity and feedback parameters during the historical period. *Geophysical Research Letters*, *43*(8), 3911–3920. doi: https://doi.org/10.1002/2016GL068406

Huang, Y., Tan, X., & Xia, Y. (2016). Inhomogeneous radiative forcing of homogeneous greenhouse gases. *Journal of Geophysical Research: Atmospheres*, *121*(6), 2780–2789. doi: 10.1002/2015JD024569

Ingram, W. (2010). A very simple model for the water vapour feedback on climate change. *Quarterly Journal of the Royal Meteorological Society*, *136*(646), 30–40. doi: 10.1002/qj.546

Jeevanjee, N., Seeley, J., Paynter, D., & Fueglistaler, S. (2020). An Analytical Model for CO_2 Forcing, Part II: State-Dependence and Spatial Variations. *Earth and Space Science Open Archive*, 47. Retrieved from `https://doi.org/10.1002/essoar.10503404.1` doi: 10.1002/essoar.10503404.1

Kasting, J. F. (1988, June). Runaway and moist greenhouse atmospheres and the evolution of Earth and Venus. *Icarus*, *74*(3), 472–494. doi: 10.1016/0019-1035(88)90116-9

Kluft, L., Dacie, S., & Bourdin, S. (2021, January). *atmtools/konrad: Add the possibility to perturb the relative humidity distribution.* Zenodo. Retrieved from https://doi.org/10.5281/zenodo.4434837 doi: 10.5281/zenodo.4434837

Kluft, L., Dacie, S., Buehler, S. A., Schmidt, H., & Stevens, B. (2019). Re-examining the first climate models: Climate sensitivity of a modern radiative-convective equilibrium model. *Journal of Climate*, *32*(23), 8111–8125. doi: 10.1175/JCLI-D-18-0774.1

Koll, D. D. B., & Cronin, T. W. (2018). Earth's outgoing longwave radiation linear due to h2o greenhouse effect. *Proceedings of the National Academy of Sciences*, *115*(41), 10293–10298. doi: 10.1073/pnas.1809868115

Kutzbach, J. E., He, F., Vavrus, S. J., & Ruddiman, W. F. (2013). The dependence of equilibrium climate sensitivity on climate state: Applications to studies of climates colder than present. *Geophysical Research Letters*, *40*(14), 3721–3726. doi: https://doi.org/10.1002/grl.50724

Manabe, S., & Bryan, K. (1985). CO2-induced change in a coupled ocean-atmosphere model and its paleoclimatic implications. *Journal of Geophysical Research: Oceans*, *90*(C6), 11689–11707. doi: https://doi.org/10.1029/JC090iC06p11689

Meraner, K., Mauritsen, T., & Voigt, A. (2013). Robust increase in equilibrium climate sensitivity under global warming. *Geophysical Research Letters*, *40*(22), 5944–5948. doi: 10.1002/2013GL058118

Minschwaner, K., & Dessler, A. E. (2004). Water vapor feedback in the tropical upper troposphere: Model results and observations. *Journal of Climate*, *17*, 1272–1282. doi: 10.1175/1520-0442(2004)017⟨1272:WVFITT⟩2.0.CO;2

Mlawer, E. J., Payne, V. H., Moncet, J.-L., Delamere, J. S., Alvarado1, M. J., & Tobin, D. C. (2012). Development and recent evaluation of the MT_CKD model of continuum absorption. *Philosophical Transactions of the Royal Society A*, *370*(1968), 2520–2556. doi: 10.1098/rsta.2011.0295

Mlawer, E. J., Taubman, S. J., Brown, P. D., Iacono, M. J., & Clough, S. A. (1997). Radiative transfer for inhomogeneous atmospheres: RRTM, a validated correlated-k model for the longwave. *Journal of Geophysical Research*, *102*, 16663–16682.

Nakajima, S., Hayashi, Y., & Abe, Y. (1992). A Study on the "Runaway Greenhouse Effect" with a One-Dimensional Radiative–Convective Equilibrium Model. *Journal of the Atmospheric Sciences*, *49*(23), 2256–2266. Retrieved from https://journals.ametsoc.org/view/journals/atsc/49/23/1520-0469_1992_049_2256_asotge_2_0_co_2.xml doi: 10.1175/1520-0469(1992)049⟨2256:ASOTGE⟩2.0.CO;2

Polya, G. (1962). *How to solve it.* Princeton University Press.

Popke, D., Stevens, B., & Voigt, A. (2013). Climate and climate change in a radiative-convective equilibrium version of echam6. *Journal of Advances in Modeling Earth Systems*, *5*(1), 1–14. doi: 10.1029/2012MS000191

Popp, M., Schmidt, H., & Marotzke, J. (2015, 01). Initiation of a Runaway Greenhouse in a Cloudy Column. *Journal of the Atmospheric Sciences*, *72*(1), 452–471. Retrieved from https://doi.org/10.1175/JAS-D-13-047.1

Romps, D. M. (2020). Climate Sensitivity and the Direct Effect of Carbon Dioxide in a Limited-Area Cloud-Resolving Model. *Journal of Climate*, *33*(9), 3413–3429. Retrieved from https://doi.org/10.1175/JCLI-D-19-0682.1 doi: 10.1175/JCLI-D-19-0682.1

Seeley, J. T., & Jeevanjee, N. (2021). H_2O Windows and CO_2 Radiator Fins: A Clear-Sky Explanation for the Peak in Equilibrium Climate Sensitivity. *Geophysical Research Letters*, *48*(4), e2020GL089609. Retrieved from https://agupubs.onlinelibrary.wiley.com/doi/abs/10.1029/2020GL089609 doi: https://doi.org/10.1029/2020GL089609

Simpson, S. G. C. (1928). *Some studies in terrestrial radiation.* Edward Stanford.

Stevens, B., & Bony, S. (2013). Water in the atmosphere. *Physics Today*, *66*(6). doi: 10.1063/PT.3.2009

Wing, A. A., Reed, K. A., Satoh, M., Stevens, B., Bony, S., & Ohno, T. (2017). Radiative-convective equilibrium model intercomparison project. *Geoscientific Model Development Discussions*, *2017*, 1–34. doi: 10.5194/gmd-2017-213

Zelinka, M. D., Myers, T. A., McCoy, D. T., Po-Chedley, S., Caldwell, P. M., Ceppi, P., . . . Taylor, K. E. (2020). Causes of Higher Climate Sensitivity in CMIP6 Models. *Geophysical Research Letters*, *47*(1). doi: https://doi.org/10.1029/2019GL085782

Figure 4.

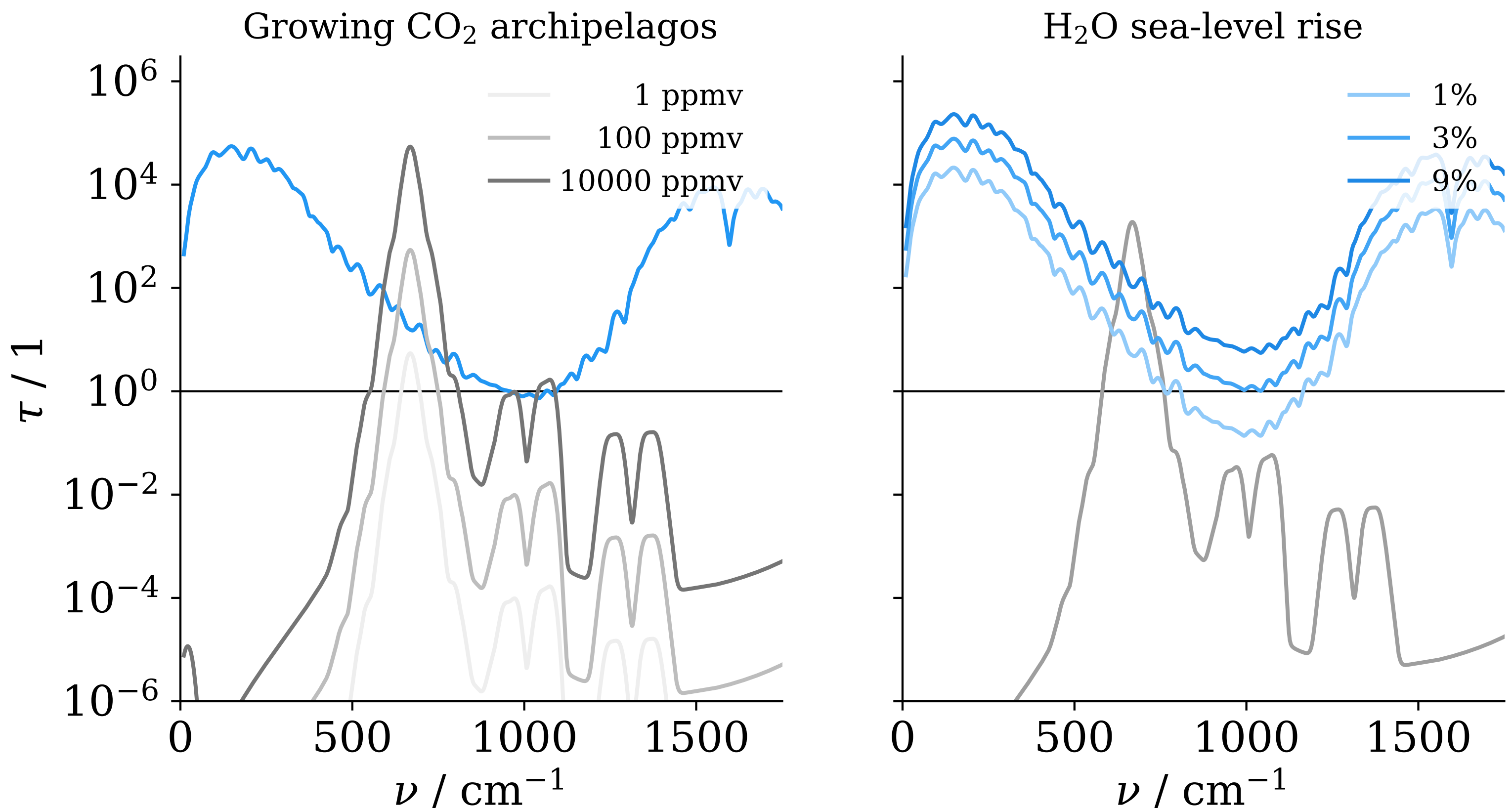

Growing CO_2 archipelagos
H_2O sea-level rise
τ / 1
10^6
10^4
10^2
10^0
10^{-2}
10^{-4}
10^{-6}
1 ppmv
100 ppmv
10000 ppmv
1%
3%
9%
0
500
1000
1500
ν / cm^{-1}

Figure 2.

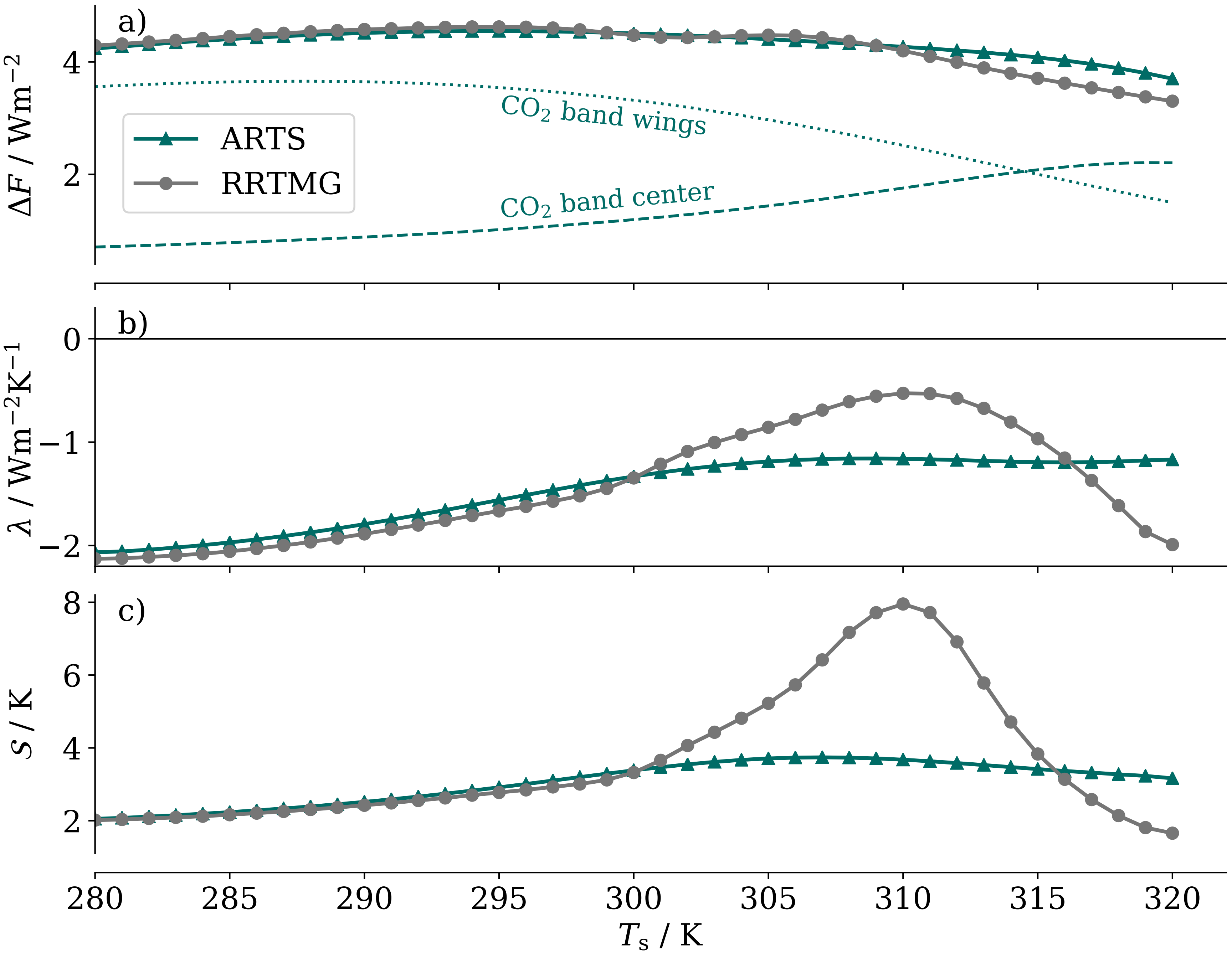

a)
b)
c)
ARTS
RRTMG
CO_2 band wings
CO_2 band center
ΔF / Wm^{-2}
λ / Wm^{-2}K^{-1}
S / K
T_s / K

Figure 1.

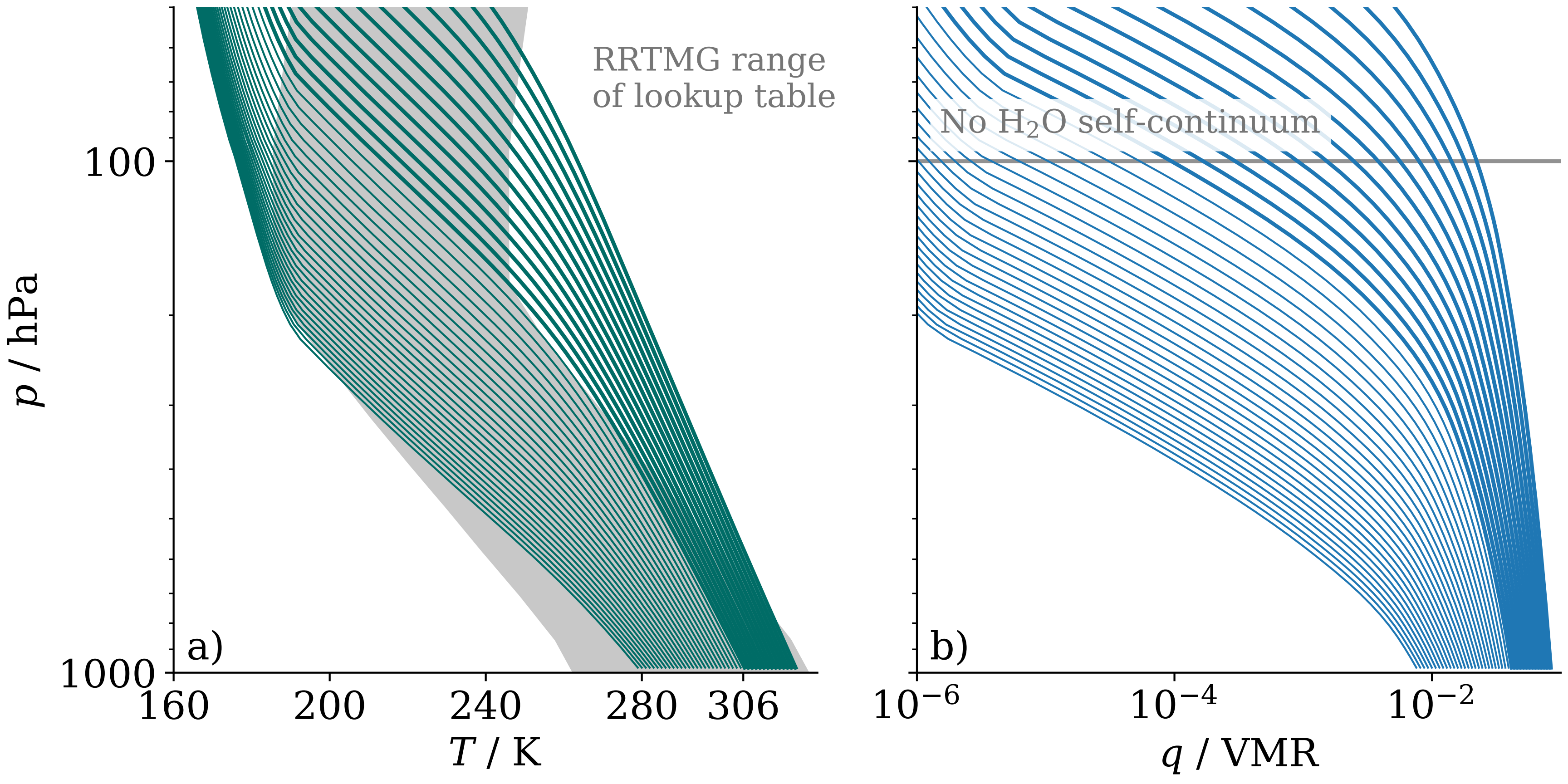

RRTMG range
of lookup table
No H_2O self-continuum
p / hPa
100
1000
160
200
240
280
306
T / K
a)
b)
10^{-6}
10^{-4}
10^{-2}
q / VMR

Figure 3.

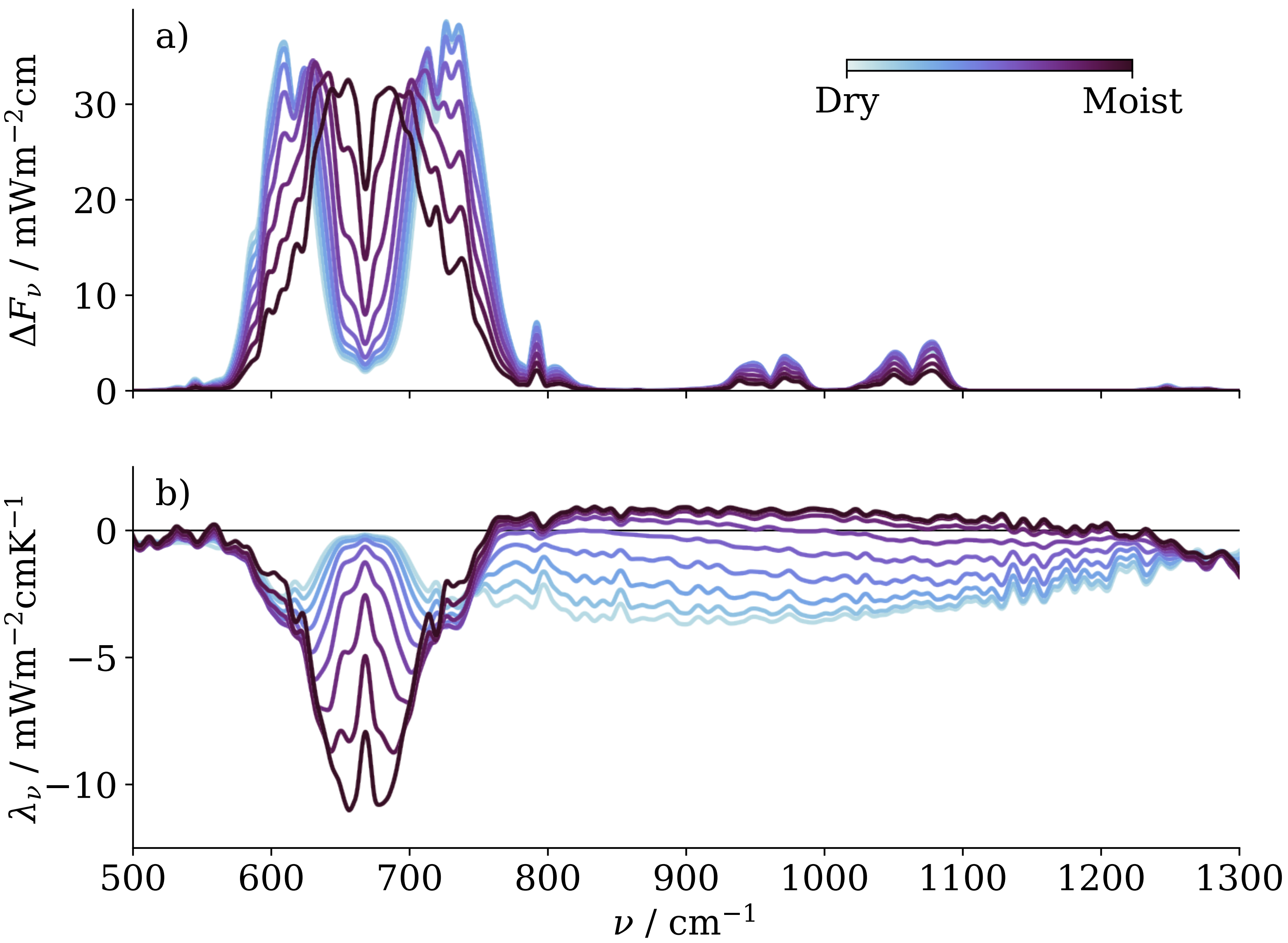

a)
Dry
Moist
ΔF_ν / mWm^{-2}cm
0
10
20
30
b)
λ_ν / mWm^{-2}cmK^{-1}
0
−5
−10
500
600
700
800
900
1000
1100
1200
1300
ν / cm^{-1}